Atmos. Meas. Tech. Discuss., 7, 12481–12515, 2014
www.atmos-meas-tech-discuss.net/7/12481/2014/
doi:10.5194/amtd-7-12481-2014

Atmospheric Measurement Techniques Discussions
Open Access

The Ice Selective Inlet: a novel technique for exclusive extraction of pristine ice crystals in mixed-phase clouds

P. Kupiszewski[1], E. Weingartner[1,*], P. Vochezer[2], A. Bigi[3], B. Rosati[1], M. Gysel[1], M. Schnaiter[2], and U. Baltensperger[1]

[1]Laboratory of Atmospheric Chemistry, Paul Scherrer Institute, Villigen PSI, Switzerland
[2]Institute for Meteorology and Climate Research, Karlsruhe Institute of Technology, Karlsruhe, Germany
[3]Department of Engineering "Enzo Ferrari", University of Modena and Reggio Emilia, Modena, Italy
[*]now at: Institute for Aerosol and Sensor Technology, University of Applied Sciences, Windisch, Switzerland

Received: 19 November 2014 – Accepted: 22 November 2014
– Published: 12 December 2014

Correspondence to: E. Weingartner (ernest.weingartner@fhnw.ch)

Published by Copernicus Publications on behalf of the European Geosciences Union.

Abstract

Climate predictions are affected by high uncertainties partially due to an insufficient knowledge of aerosol-cloud interactions. One of the poorly understood processes is formation of mixed-phase clouds (MPCs) via heterogeneous ice nucleation. Field measurements of the atmospheric ice phase in MPCs are challenging due to the presence of supercooled liquid droplets. The Ice Selective Inlet (ISI), presented in this paper, is a novel inlet designed to selectively sample pristine ice crystals in mixed-phase clouds and extract the ice residual particles contained within the crystals for physical and chemical characterisation. Using a modular setup composed of a cyclone impactor, droplet evaporation unit and pumped counterflow virtual impactor (PCVI), the ISI segregates particles based on their inertia and phase, exclusively extracting small ice particles between 5 and 20 µm in diameter. The setup also includes optical particle spectrometers for analysis of the number size distribution and shape of the sampled hydrometeors.

The novelty of the ISI is a droplet evaporation unit, which separates liquid droplets and ice crystals in the airborne state, thus avoiding physical impaction of the hydrometeors and limiting potential artifacts. The design and validation of the droplet evaporation unit is based on modelling studies of droplet evaporation rates and computational fluid dynamics simulations of gas and particle flows through the unit. Prior to deployment in the field, an inter-comparison of the WELAS optical particle size spectrometers and a characterisation of the transmission efficiency of the PCVI was conducted in the laboratory. The ISI was subsequently deployed during the Cloud and Aerosol Characterisation Experiment (CLACE) 2013 – an extensive international field campaign encompassing comprehensive measurements of cloud microphysics, as well as bulk aerosol, ice residual and ice nuclei properties. The campaign provided an important opportunity for a proof of concept of the inlet design. In this work we present the setup of the ISI, including the modelling and laboratory characterisation of its components,

AMTD

7, 12481–12515, 2014

as well as a case study demonstrating the ISI performance in the field during CLACE 2013.

1 Introduction

High uncertainties in future climate predictions arise from insufficient knowledge of the interaction of clouds with visible (solar) and infrared (terrestrial) radiation. The optical properties, cloud lifetime and cloud cover are strongly influenced by the ability of atmospheric aerosol particles to act as cloud condensation nuclei (CCN) or ice nuclei (IN) (Lohmann and Feichter, 2005; Penner, 2004). These aerosol-cloud interactions have been recognized as the greatest sources of uncertainty in the anthropogenic effective radiative forcing (Myhre et al., 2013) and, thus, in assessing human impact on climate. Up to now, the climate relevant properties of clouds and their formation processes are still poorly understood, particularly those of mixed-phase clouds where supercooled liquid droplets and ice crystals coexist. Previous research has found that the cloud radiative properties strongly depend on the cloud ice mass fraction (Sun and Shine, 1994), which is influenced by the abundance of IN. Increased IN concentrations are also thought to enhance precipitation (Chen and Lamb, 1999; Pruppacher and Klett, 1997), thus causing a decrease in cloud lifetime and cloud cover, and affecting the radiative budget of the atmosphere (Lohmann and Feichter, 2005). Meanwhile, the physical and chemical properties of atmospherically relevant IN are not well known. For example, it is unclear whether anthropogenic emissions of black carbon (BC) contribute significantly to IN number, besides natural IN such as mineral dust or bacteria. Field measurements have not been conclusive as to the role of BC. For example, based on measurements at the high alpine research station Jungfraujoch, Cozic et al. (2008) found enrichment of BC in ice residuals (IR) extracted from small ice crystals, while Chou et al. (2011) found no correlation between IN number concentration and BC mass concentration. Should BC be an atmospherically important IN, the increase in aerosol concentrations since pre-industrial times would be responsible for a glacia-

AMTD
7, 12481–12515, 2014

tion indirect effect on clouds. Cloud glaciation would be more frequent in present-day times, resulting in a higher precipitation probability of a cloud (due to the rapid growth of ice crystals at the expense of supercooled droplets via the Wegener–Bergeron–Findeisen process). This in turn would have reduced the cloud fraction, thus leading to an increase in absorption of shortwave radiation by the Earth-atmosphere system (Lohmann, 2002).

The interaction between aerosols and mixed-phase clouds (MPCs) is presently poorly understood and field studies on the physical and chemical characteristics of IN are sparse (Cantrell and Heymsfield, 2005). A number of studies on IR properties have been conducted in high-altitude ice clouds using a counterflow virtual impactor (CVI) to separate interstitial aerosol particles and ice crystals (e.g., Cziczo et al., 2013; Prenni et al., 2007; Twohy and Poellot, 2005). However, field measurements of ice residuals in mixed-phase clouds are hampered by difficulties with extracting the relatively few ice crystals found in MPCs and separating them from the much more numerous supercooled liquid droplets. This challenge is further exacerbated by the fact that small, freshly nucleated ice crystals have similar aerodynamic diameters to the liquid cloud droplets, and thus cannot be separated using conventional impactor techniques. To the best of the authors' knowledge, prior to this work only one ground-based inlet for sampling ice crystals in MPCs has been successfully operated and described in literature. This so-called Ice Counterflow Virtual Impactor (Ice-CVI) (Mertes et al., 2007) employs a series of modules to remove precipitating particles, particles larger than 20 µm, supercooled droplets and interstitial particles. Separation of the liquid and ice phases is achieved using a two-stage impactor consisting of cool plates on which hydrometeors are impinged. Upon impact the droplets freeze on the surface of the plate, while the ice crystals bounce off.

In view of the difficulties in measurements of the ice phase in MPCs, the paucity of inlet systems suitable for MPC measurements, and the resulting scarcity of data from the field, there is a great need for development of novel instrumentation. In this paper we describe the Ice Selective Inlet (ISI) which is designed and developed to extract ice crystals in MPCs and is conceptually inspired by the Ice-CVI (Mertes et al., 2007). The ISI separates small pristine ice particles (their residuals are considered representative of the original IN) from supercooled liquid droplets, interstitial particles and potentially contaminated large ice crystals, and extracts the ice residuals contained within the small ice crystals for physical and chemical characterisation. The inlet represents a novel tool for the in-situ investigation of MPCs and the optical particle spectrometers contained within the inlet deliver information that is not available by means of any other existing inlet. The ISI has been successfully deployed and tested in the field for the first time as part of the Cloud and Aerosol Characterisation Experiment (CLACE) 2013 – an international campaign encompassing comprehensive measurements of cloud microphysics, as well as bulk aerosol, ice residual and ice nuclei properties. In this work we present the setup of the ISI, including the modelling and laboratory characterisation of its components, as well as a case study demonstrating the ISI performance in the field during CLACE 2013.

2 Setup and characterisation of the Ice Selective Inlet

2.1 Ice Selective Inlet setup

The design of the Ice Selective Inlet (Fig. 1) is inspired by the Ice-CVI inlet (Mertes et al., 2007), albeit with some key differences. Foremost amongst these is the technique used to separate ice crystals from supercooled droplets. In the ISI the separation takes place in the airborne state, as opposed to physical impaction on cool plates, thus limiting potential artifacts, e.g., from ice crystal break-up or abrasion of the inlet surface coating. The working principle of the droplet evaporation unit, which is used to remove supercooled liquid droplets sampled by the ISI, is described in detail in Sect. 2.2. Other components of the ISI are described as follows: Cloud air is aspirated through the ISI at a rate of $7\,\mathrm{L\,min^{-1}}$. An omnidirectional inlet, shielded from above and a custom-made Sharp Cut Cyclone (BGI Inc., USA), with a D_{50} (i.e. the aerodynamic diameter

AMTD
7, 12481–12515, 2014

at which 50 % of the particles are removed from the sample flow and 50 % are transmitted) of 20 µm ensure that precipitating particles and ice crystals larger than 20 µm in aerodynamic diameter are removed from the sample flow. It is important to remove the larger ice particles because the residuals contained within larger ice crystals may be unrepresentative of the original ice nuclei. The larger ice crystals have not necessarily grown by water vapour diffusion, as is assumed for small ice crystals; instead they may have grown by riming (i.e. capture and freezing of supercooled liquid droplets on falling ice crystals (Mosimann et al., 1994) and thus they could also contain CCN. Furthermore, uptake of gases on ice crystals may take place (e.g., Kärcher and Basko, 2004; Marécal et al., 2010), thus contaminating the ice residuals. Larger, more aged ice particles would be more susceptible to contamination via this pathway than small, fresh ice crystals.

Hydrometeor number size distributions are measured upstream and downstream of the droplet evaporation unit using two WELAS 2500 aerosol sensor systems (white-light aerosol spectrometer; Palas GmbH, Germany). Each sensor system contains a WELAS 2500 sensor and a Promo 2000 control unit. The latter houses the white light source and a photomultiplier tube (PMT) where the light scattered at an angle of 78–102° by particles passing through the sensing volume is measured. Optical fibres are used to transmit light between the Promo 2000 and the WELAS 2500. The use of white light is important in helping to circumvent difficulties in particle sizing which arise when using a laser spectrometer due to the strongly non-monotonic relationship between the intensity of scattered light and particle diameter (Heim et al., 2008). Furthermore, decoupling of the light source from the measuring volume using optical fibres is an important feature which prevents heat transfer to the ISI system. For an in-depth and extensive description of the measurement principle of WELAS sensors the reader is referred to Heim et al. (2008) and Rosati et al. (2014).

Downstream of the WELAS sensors the PPD-2K, a modified version of the Particle Phase Discriminator (Kaye et al., 2008), custom-built and adapted for use within the ISI inlet, is mounted. The modifications of the PPD-2K compared to the instrument described in Kaye et al. (2008) are the replacement of the in-board PC by an external laptop and the use of polyether ether ketone (PEEK) encapsulations for the inlet and outlet nozzle of the instrument. With these modifications the heat transfer to the sample flow is minimized and the operation of a computer under harsh conditions is avoided. The PPD-2K acquires high resolution scattering patterns of individual cloud particles. In order to calibrate the sizing of the instrument, scattering patterns of droplets are selected and exact Mie solutions are fitted to these patterns. Thus, the PPD-2K provides an optical diameter which is equivalent to the scattering of a droplet in 5–26° forward direction. The scattering patterns contain information about microphysical properties of individual cloud particles such as particle size, shape and surface roughness. Thus, the analysis of the PPD-2K scattering patterns enables a highly sensitive distinction between water droplets and ice particles and provides an invaluable check of the droplet evaporation unit operation. The scattering patterns are recorded starting from the detection limit of around 5 µm. The analysis procedure will be the subject of a separate publication (Vochezer et al., 2014). In addition to the scattering patterns the PPD-2K generates a particle number size distribution based on the forward scattering signal.

Downstream of the PPD-2K, interstitial particles and residual particles released from the droplets in the droplet evaporation unit are removed from the sample flow with the use of the commercially available pumped counterflow virtual impactor (PCVI, model 8100, Brechtel Manufacturing Inc. (USA); Boulter et al., 2006; Kulkarni et al., 2011) which separates particles based on their inertia. Particles with insufficient inertia to overcome a counterflow are removed while particles above a certain aerodynamic cut size are transmitted. Further details on characterisation of the PCVI transmission efficiency can be found in Sect. 2.4. The ice crystals extracted with the PCVI are subsequently evaporated and the physical and chemical properties of the ice residuals can be probed using on- and off-line aerosol instrumentation.

AMTD
7, 12481–12515, 2014

Title Page
Abstract | Introduction
Conclusions | References
Tables | Figures
◀| |▶
◀ ▶
Back | Close
Full Screen / Esc
Printer-friendly Version
Interactive Discussion

2.2 Working principle of the droplet evaporation unit

The phase separation in the ISI is accomplished with the use of a droplet evaporation unit. The unit is an anodized aluminium chamber with sandblasted inner walls and a volume of 29 L split in twelve axially symmetrical parts. During operation, the inner walls of the chamber are coated with ice (it should be noted that the temperature of the droplet evaporation unit is not actively controlled, i.e., it follows the ambient air temperature). As a result the air within the chamber is saturated with respect to a flat ice surface, resulting in evaporation of droplets using the Wegener–Bergeron–Findeisen process. This process takes place due to the different saturation vapour pressures over liquid water and ice (Fig. 2; the parametrisations used for the saturation vapour pressures over water and ice are based on Lowe and Ficke, 1974). Consequently, at a given temperature, in an environment saturated with respect to ice (green curve in Fig. 2), there is sub-saturation with respect to water, i.e. the ambient water vapour pressure is below the saturation vapour pressure with respect to water (blue curve in Fig. 2). This difference in saturation vapour pressures over water and ice (red curve in Fig. 2) induces evaporation of the super-cooled droplets, while ice crystals are affected to a much lesser degree.

As the temperature of the droplet evaporation unit is not actively controlled, it is possible that there is a slight lag in temperature equilibration of the chamber walls relative to the ambient temperature. In order to monitor whether such a lag takes place, the air temperature inside the evaporation unit and the wall temperature of the chamber were monitored using PT100 (platinum temperature resistance detector) probes. Absolute differences in temperature were on average approximately 0.25 °C. In order to show the influence of such a temperature lag on the driving force behind the Wegener-Bergeron-Findeisen process we show the difference in saturation vapour pressures over water and ice when the ice temperature is 0.25 °C higher and lower (dashed and dotted red lines respectively in Fig. 2) than the droplet temperature (the droplet temperature is assumed to be equal to the ambient air temperature).

AMTD
7, 12481–12515, 2014

The design of the droplet evaporation unit is based on model calculations solving mass transfer equations and Köhler theory, ensuring sufficient residence time for evaporation of the droplets. The mass transfer equation used follows Seinfeld and Pandis (2006) and gives the growth/evaporation rate of a solution droplet as follows:

$$D_p \frac{\mathrm{d}D_p}{\mathrm{d}t} = \frac{S_{\mathrm{v},\infty} - S_{\mathrm{eq}}}{\frac{\rho_\mathrm{w} R T_\infty}{4 p_\mathrm{s}(T_\infty) D'_\mathrm{v} M_\mathrm{w}} + \frac{\Delta H_\mathrm{v} \rho_\mathrm{w}}{4 k'_\mathrm{a} T_\infty}\left(\frac{\Delta H_\mathrm{v} M_\mathrm{w}}{T_\infty R} - 1\right)} \quad (1)$$

Where D_p is the droplet diameter, $S_{\mathrm{v},\infty}$ the ambient water vapour saturation ratio, S_{eq} the equilibrium water vapour saturation ratio of the droplet, ρ_w the density of water, R the ideal gas constant, T_∞ the ambient temperature, p_s the saturation vapour pressure of water, D'_v the water vapour diffusivity corrected for non-continuum effects, M_w the molecular weight of water, k'_a the thermal conductivity of air accounting for non-continuum effects and ΔH_v the latent heat of water evaporation.

Rearrangement and integration of Eq. (1) gives:

$$\int_{D_0}^{D_1} \frac{1}{\frac{S_{\mathrm{v},\infty} - S_{\mathrm{eq}}}{\frac{\rho_\mathrm{w} R T_\infty}{4 p_\mathrm{s}(T_\infty) D'_\mathrm{v} M_\mathrm{w}} + \frac{\Delta H_\mathrm{v} \rho_\mathrm{w}}{4 k'_\mathrm{a} T_\infty}\left(\frac{\Delta H_\mathrm{v} M_\mathrm{w}}{T_\infty R} - 1\right)}} D_p \mathrm{d}D_p = \int_{t_0}^{t_1} \mathrm{d}t \quad (2)$$

Using the MATLAB R2014a (The Mathworks Inc., USA) software package, Eq. (2) was solved by numeric integration to give the time needed to evaporate a droplet from a set start to a set end diameter, as a function of temperature (Fig. 3). The ambient water vapour saturation ratio was assumed to be at 100 % saturation with respect to a flat ice surface ($\mathrm{RH_{ice}} = 100\,\%$), the ambient pressure p was set to 658.61 hPa (in order to simulate the ambient conditions at the Jungfraujoch), the equilibrium water vapour saturation ratio of the droplet S_{eq} was assumed to be 1 (i.e., the Kelvin and Raoult effect are negligible for supermicron sized cloud droplets) and the mass accommodation coefficient (a component of the D'_v term) was set to 1. A sensitivity analysis of the importance of the mass accommodation coefficient was additionally performed by setting it to 0.1 and 0.01 for the evaporation time calculations of droplets with a set start diameter of 20 µm. In order to check whether droplet residence times would be sufficient to allow droplet evaporation in the unit, the average residence time as a function of temperature for a 20 µm droplet was calculated based on the dimensions of the droplet evaporation unit and a sample flow of 7 L min^{-1}. The dotted black line in Fig. 3 shows the average residence time in the evaporation unit.

The calculations of droplet evaporation times based on the aforementioned parameters show that droplets with diameters of 10 µm take a few seconds to evaporate to a diameter of 3 µm, a size well below the cut-off of the PCVI, while 20 µm droplets need approximately ten to twenty seconds and 50 µm droplets need on the order of one hundred seconds (Fig. 3). As seen in Fig. 3, there are significant differences in the evaporation rate depending on temperature. Droplet evaporation takes longest at near-zero temperatures, as well as towards the lower limit of the modelled temperature range, with evaporation times increasing as temperature drops below −14 °C. The fastest evaporation rates are at a temperature of approximately −12 to −14 °C. These dependencies can be explained by the difference in saturation vapour pressures over water and ice as a function of temperature (red curve in Fig. 2): the difference is lowest at near-zero and at very low temperatures, and highest between −10 and −15 °C. The difference in saturation vapour pressures between water and ice is the driving force for the Wegener–Bergeron–Findeisen process. Consequently, where the difference and, therefore, driving force is highest, evaporation rate is at its fastest, and vice-versa.

A potentially important uncertainty in the modelled evaporation times arises due to the uncertainties associated with the assumed mass accommodation coefficient value. Many conflicting studies exist on the value of the mass accommodation coefficient, also called the condensation or evaporation coefficient. Moreover, while some studies assume the condensation and evaporation coefficient to be synonymous (e.g., Fukuta and Walter, 1970; Shaw and Lamb, 1999), other studies highlight that the two coefficients are distinct and can have different values (Eames et al., 1997; Marek and Straub, 2001; Pound, 1972). A review of experimental studies investigating evaporation coef-

AMTD
7, 12481–12515, 2014
The Ice Selective Inlet
P. Kupiszewski et al.

ficients conducted by Eames et al. (1997) demonstrates the lack of agreement with wide-ranging values between 0.01 and 1 found in different studies. More recent studies slightly narrow this range to 0.04 and 1 (Laaksonen et al., 2005) (with no differentiation however between the condensation and evaporation coefficients), while aerosol/cloud models have employed values between 0.042 and 1 for the condensation coefficient when modelling droplet growth (Kreidenweis et al., 2003).

While it is outside the scope of this paper to investigate the mass accommodation coefficient of water, we incorporate a simple sensitivity analysis of the mass accommodation coefficient into the modelling study of droplet evaporation rates in order to establish its potential impact on the evaporation rates. The sensitivity analysis is carried out for evaporation of droplets with a set start diameter of 20 µm and shows that a decrease in the mass accommodation coefficient by one order of magnitude would result in an increase in the evaporation time of a 20 µm droplet by 17–26 %. A decrease in the mass accommodation coefficient by two orders of magnitude would result in the droplet evaporation time increasing by 183–288 %, depending on the temperature. Meanwhile the residence time of a 20 µm droplet in the evaporation unit was calculated to be over 200 s for temperatures between −2 and −30 °C. This means that residence time in the droplet evaporation unit should be more than sufficient to ensure evaporation of 20 µm droplets. It is important to note that the modelled conditions of 20 µm droplet diameter are a worst case scenario, as droplet sizes are usually significantly below 20 µm diameter (e.g., Choularton et al., 2008) and, furthermore, hydrometeors larger than this should be removed by the cyclone.

As regards the geometry of the droplet evaporation unit, an internal structure was designed, as shown in Fig. 4. The internal structure provides a greater inner ice-covered surface, as well as homogenising the velocity of the sampled air through the droplet evaporation unit (thus slowing down droplet transport and allowing more time for droplet evaporation). Due to the radial construction of the structure, the flow velocity is decreased in the center of the droplet evaporation unit; the distances between wall surfaces here are smallest resulting in friction between the sample air and chamber

AMTD
7, 12481–12515, 2014

walls impacting the air flow velocity to a greater extent than further from the center of the chamber. As the cone at the centre of the structure forms a surface for potential impaction of hydrometeors, the geometry of the unit was modelled and computational fluid dynamics (CFD) simulations were conducted using the Comsol Multiphysics 4.2a software (Comsol Inc., USA). It should be noted that the geometry used for the CFD modelling is simplified and does not incorporate the internal radial structure, but only the center cone itself. A visualisation of the CFD simulation results, namely a 2-D cross-section of the droplet evaporation unit showing the air streamlines and velocity field, is presented in Fig. 5. The Comsol particle tracing module was used in order to model particle transport through the chamber and to establish whether particle losses could be of concern. The simulation was initiated by injecting spherical particles with an aerodynamic diameter of 20 µm into the chamber. As in the case of the calculated droplet residence time in the evaporation unit, the simulation was conducted based on the worst case scenario, with injection of 20 µm particles which have a higher stopping distance than smaller particles and are thus more likely to impact on the internal structure, as opposed to following the gas streamlines. The CFD simulations of particle trajectories through the droplet evaporation unit showed impaction of large particles to be of minimal importance. Furthermore, the gas flow streamlines simulated show a smooth flow of air through the unit, with only minor eddy formation (which could lead to particle losses if significant) in the upper cone due to an increase in diameter of the sample flow conduit as the flow enters the evaporation tube and is transported through its upper section (Fig. 5).

2.3 WELAS sensor characterisation

The raw signal measured by the WELAS sensors and subsequently converted to a particle number size distribution is voltage. An empirical factory calibration is used to relate the measured voltage to particle size. The empirical calibration combined with Mie theory provides a relationship in turn between voltage and particle scattering cross section (the latter is directly proportional to the voltage). In order to correct for any drift in instrument sensitivity due to e.g. degradation in the light source or optical fibres, contamination of the optical windows or changes in performance of the photomultiplier a user calibration is conducted. Hereby particles with a known scattering cross section are aspirated through the measuring volume of the WELAS, with a flow rate of $7\,\mathrm{L\,min^{-1}}$, and the calibration factor is empirically established. CalDust 1100 (provided by the manufacturer), a calibration dust with a refractive index (RI) of 1.43, and a diameter of 1.1 µm is used for this purpose. The WELAS sensors are calibrated assuming an RI of 1.59, therefore the calibration factor is adjusted so that the measured size of the mono-disperse CalDust is 0.85 µm (i.e. the optical diameter of the CalDust particles when assuming they have an RI of 1.59). As the RI of liquid water is 1.33, Mie theory (e.g., Bohren and Huffman, 2007) is subsequently used to correct the measured size distributions for the RI of liquid water. The calculations are conducted with the assumption that the measured particles are spherical. It is important to note that as a result of a single RI being used for the size distribution correction the diameters calculated are incorrect for particles with a different RI, i.e., non-activated aerosol particles and ice crystals. Nonetheless, hydrometeor measurements are the focus of the study, and droplets make up the vast bulk of the hydrometeors measured upstream of the droplet evaporation unit, therefore this approach is deemed satisfactory. A further point to make is that as ice crystals are highly aspherical, they can only be counted, and not accurately sized, by the WELAS sensors; the shape and orientation of ice crystals in the measuring volume of the WELAS sensor are unknown, both of which affect the intensity of scattered light.

The two WELAS 2500 sensors used within the ISI and the respective Promo 2000 control units are, in theory, identical models. Nonetheless, as with all scientific instruments, due to possible slight differences in the machining, assembly and calibration of any two such devices, differences in instrument performance are commonplace. Consequently, we have performed a laboratory characterisation of the two WELAS sensors in order to establish the potential error in subsequent comparisons of ambient measurements. The experiment was conducted as follows: The instruments were set up

AMTD
7, 12481–12515, 2014

side-by-side and sampled simultaneously via a common inlet followed by a Y-splitter. A3 medium grade Arizona Test Dust (ISO 12103-1; Powder Technology Inc, USA) was used as the test aerosol. The aerosol was dispersed using a vial shaker (Edmund Bühler GmbH, Germany). The WELAS sensors measured the number size distribution of the sampled aerosol in the PSL-equivalent size range of approximately 0.6–40 µm. Using Mie theory, the measured size distributon was corrected for particles with the refractive index of Arizona Test Dust (the RI across the WELAS effective light spectrum is assumed to have real and imaginary parts of $n = 1.51$ and $k = 0.0012$ respectively, as given by Glen and Brooks, 2013).

The size distributions measured during the instrument characterisation are presented in Fig. 6, together with the ratio of the total number of counts per size bin measured by the two sensors (red line in Fig. 6). The ratio shows that there are considerable differences in the relative counting efficiencies of the two sensors at the smallest sizes with the ratio of WELAS 2 to WELAS 1 counts steadily increasing from 20 % to just under 100 % for 0.5 to 1 µm particles. The relative counting efficiency is in fairly good agreement for particles between 0.8 and 11 µm, albeit with WELAS 2 predominantly under-counting by 10–20 % as compared to WELAS 1. Above 11 µm the ratio of counts increases considerably in the experiment shown.

The *S*-shape of the ratio of Welas 2 to Welas 1 counts could be explained by a difference or an inherent uncertainty in the CalDust user calibration. An over-amplification of the signal for Welas 2 (or an under-amplification for Welas 1) would result in a relative shift in the measured size distribution of Welas 2 towards larger sizes, thus resulting in under-counting of Welas 2 with respect to Welas 1 where the gradient of the size distribution is positive and over-counting where the gradient is negative (as observed during the experiment). Additionally, the larger differences in counting efficiencies measured at smaller sizes can be explained by the fact that at these sizes there is relatively little scattered light reaching the WELAS detector. As a result, any differences in construction or calibration of the sensors will have an increasingly strong influence on particles as their size decreases towards the lower detection limit of the WELAS sensors. This

AMTD
7, 12481–12515, 2014

could be considered an issue for some measurement purposes, however, as we are interested in supermicron sized hydrometeors, it does not pose a major problem for measurements of droplets and ice crystals in the ISI. Nonetheless the inter-comparison shows that a systematic error of up to approximately 20 % should be recognised when discussing further results of the WELAS measurements.

2.4 PCVI characterisation

A defining characteristic of an impactor device is its size dependent transmission efficiency (TE), particularly the D_{50}. Characterization of the PCVI transmission efficiency has been performed in several previous studies (Boulter et al., 2006; Kulkarni et al., 2011). As a result, we have focused solely on validating the characterisation for those flow settings that were deemed relevant to our inlet setup.

The characterisation performed within the scope of this study was carried out via dispersion of ATD as the test aerosol, as opposed to the nebulisation of salt solutions used in previous studies. In order to establish the size dependent TE, the following laboratory experiment was conducted (see Fig. 7 for a schematic of the laboratory setup): Arizona Test Dust was dispersed with the use of the Topas Solid Aerosol Generator (SAG 410; Topas GmbH, Germany). In order to smooth concentration fluctuations due to changes in the output rate of the SAG, the flow was passed through a mixing chamber before being sent either through the PCVI or through a bypass. A three-way valve was used to switch between PCVI and bypass in alternating cycles of 30 s duration. The PCVI flow settings used during the characterisation were identical to those used subsequently during the CLACE 2013 field campaign (sample flow: 7 $\mathrm{L\,min^{-1}}$, pump flow: 8.3 $\mathrm{L\,min^{-1}}$, add flow: 2.3 $\mathrm{L\,min^{-1}}$ and outlet flow: 1 $\mathrm{L\,min^{-1}}$). Number size distributions were measured downstream of the PCVI and downstream of the bypass by the TSI Aerodynamic Particle Sizer (APS), model 3321 in the size range of 0.5–20 µm aerodynamic diameter. The number size distribution measured downstream of the PCVI was corrected for enrichment in the PCVI which is approximately equal to the ratio of the inlet and outlet flow (Boulter et al., 2006). The transmission efficiency of the PCVI

AMTD
7, 12481–12515, 2014

was subsequently obtained by taking the ratio of the corrected number size distribution downstream of the PCVI to that measured downstream of the bypass.

The result of one such experiment is presented in Fig. 8. As is immediately clear, there is very little transmission of submicron particles through the PCVI (< 0.05 %). Transmission efficiency increases sharply for particles above 3.5 µm in aerodynamic diameter, with a D_{50} of 4.9 µm and the plateau value with a maximum TE of about 80 % is reached for particles larger than approximately 6 µm. This pattern is in line with the idealised TE curves derived from CFD simulations in Kulkarni et al. (2011), to which the reader is referred to for an in-depth discussion of the curve morphology. The maximum TE observed is also similar to that reported by both Boulter et al. (2006) and Kulkarni et al. (2011), with an imperfect TE being attributed to losses on the internal fittings of the PCVI. However, the D_{50} measured was consistently higher than that measured for very similar flow settings by Kulkarni et al. (2011) (Case number 5), with a D_{50} of 4.9 µm in our characterisation, as compared to 3.21 µm in Kulkarni et al. (2011). As it is of utmost importance to remove all interstitial particles from the sample flow, the higher cut-off size is not detrimental for our purposes, and based on our laboratory characterisation, the performance of the PCVI was deemed adequate.

3 First field measurements: deployment of the ISI at the Jungfraujoch

First deployment of the ISI in the field was carried out as part of an international field campaign: the Cloud and Aerosol Characterization Experiment (CLACE) 2013. The campaign was conducted at the High Alpine Research Station Jungfraujoch (3580 m a.s.l.) in the Swiss Alps. As part of the campaign, three aerosol inlets were operated (total aerosol inlet (Weingartner et al., 1999), Ice-CVI (Mertes et al., 2007) and ISI (this paper)), as well as ice nuclei counters and a host of cloud microphysical probes deployed by collaborators from Germany, the UK and Switzerland. The comprehensive set of measurements involved physical and chemical characterisation of the total aerosol, ice residuals and ice nuclei, as well as hydrometeor concentration

AMTD
7, 12481–12515, 2014

and size distribution measurements and measurements of ice crystal properties, such as shape, habit and surface roughness. Among the instruments measuring ice crystal properties was the small ice detector (SID-3, Kaye et al., 2008) which is the aircraft version of the PPD-2K, equivalent in measurement principle and output. The SID-3 directly sampled and probed the unaltered cloud and could thus be used in conjunction with the PPD-2K to assess the impact of the ISI on the ice crystals.

In this paper, only measurements of hydrometeors based on the optical particle spectrometers within the ISI are discussed in detail, with focus on validating the working principle of the droplet evaporation unit. A comparison of size distributions measured by the two WELAS sensors upstream and downstream of the droplet evaporation unit during a mixed-phase cloud measurement (19:55 LT, 12 February 2013 to 01:20 LT, 13 February 2013) is shown in Fig. 9, highlighting the strengths and weaknesses of the ISI. Results of supporting measurements from the PPD-2K are shown in Fig. 10a, with measurements from the PPD-2K mounted downstream of the AIDA cloud chamber during an ice cloud experiment and CLACE 2013 measurements from the SID-3 instrument shown for inter-comparison purposes in Fig. 10, panels b and c respectively.

Air temperature during the case study period was in the range of −20 to −22 °C (black curve in Fig. 9a), dropping gradually during this period. Liquid water content (measured by a particulate volume monitor (PVM-100, Gerber Scientific Inc., USA) fluctuated between approximately 0.1 and 0.5 $\mathrm{g\,m^{-3}}$ (blue curve in Fig. 9a). The WELAS size distributions (see Fig. 9b and d) show high concentrations of hydrometeors with a mode between approximately 2 and 11 µm. These are assumed to be predominantly supercooled droplets based on a comparison with the scattering patterns recorded by the SID-3 (not shown). The SID-3 measurements confirm also presence of ice in the cloud. The case study period was therefore a prolonged period of time during which the ISI sampled in mixed-phase cloud conditions.

In Fig. 9b and c are presented the contour plots of the 60 s time-resolved size distributions during the case study period as measured by the WELAS sensors up- and downstream of the droplet evaporation unit respectively. Figure 9d shows the case study average concentration per size bin for each sensor, along with a description of the processes occurring within the ISI and their effect on the measured size distributions. The comparison of WELAS size distributions suggests that droplets are removed very efficiently by the evaporation unit: the droplet mode clearly visible during the MPC event in the upper WELAS size distribution is removed by the ISI, as seen in the lower WELAS size distribution. The removal of droplets is confirmed by the PPD-2K measurements, which shows that the remaining hydrometeors are almost exclusively ice crystals. In the time frame selected for the case study the PPD-2K recorded 1248 scattering patterns from which 10 were classified as droplets. This corresponds to a droplet transmittance of $0.8 \pm 0.25\,\%$. The classification was based on the variance of the azimuthal intensity of the patterns (the classification method will be the subject of an upcoming publication Vochezer et al., 2014) and a manual crosscheck. The finding that the PPD-2K recorded mainly ice particles was confirmed in various cases throughout the campaign and leads to the conclusion that the dominating hydrometeors transmitted by the ISI are ice particles.

As seen in Fig. 9d, the transmitted fraction of larger particles above approximately 12 µm is much higher than of particles in the sub-11 µm range, where the droplet mode is present. Due to the rapid growth of ice crystals in the presence of supercooled liquid droplets, these larger particles are expected to be predominantly ice crystals. Although the transmitted fraction of larger particles is much higher, there are significant losses of these particles in the inlet. The PPD-2K provides important clues with regards to the process behind the imperfect transmission of the ice crystals. Figure 10a and b displays the scattering patterns recorded during CLACE 2013 by the PPD-2K (downstream of the ISI) and by the SID-3 (directly sampling ambient air) respectively. SID-3 records indicate a dominant presence of liquid droplets during the case study period, indicating that a MPC was present (note: only ice crystal scattering patterns are shown in Fig. 10b; see Kaye et al., 2008 for details on differentiating between supercooled droplets and ice crystals and examples of the respective scattering patterns). Due to the SID-3 camera trigger settings used during the case study period SID-3 data on

AMTD
7, 12481–12515, 2014

small ice particles is available only 1.5 h prior to the time period of the presented case study. The meteorological conditions however stayed rather constant and the SID-3 scattering patterns displayed in Fig. 10b are typical for the SID-3 measurements of small ice crystals during CLACE 2013.

Comparing the general features of the scattering patterns displayed in Fig. 10a and b one notes that the patterns recorded by the PPD-2K downstream of the ISI (Fig. 10a) show a more rounded structure than those measured by the SID-3 directly sampling the ambient air (Fig. 10b). This indicates that the ice particles are altered during their passage through the ISI evaporation unit. In order to explain this discrepancy the scattering patterns observed by the PPD-2K during the case study period (Fig. 10a) have been compared to those collected by the same instrument during a cloud chamber experiment: in Fig. 10c are displayed patterns recorded at the AIDA cloud chamber (e.g., Möhler et al., 2005) within an ice cloud experiment during sublimation of ice particles. Patterns in Fig. 10a and c show similar rounded features. Applying diffraction theory as a first approximation to interpret the scattering patterns we expect rounded patterns to be correlated to rounded ice particles. Thus the patterns displayed in panels a and c both suggest the presence of rounded ice particles. Together with the disappearance of particles indicated by the low transmission efficiency in Fig. 9 we suspect the ice particles to have been sublimated during their passage through the ISI evaporation chamber. Roundening of ice particles as an indicator of ice crystal sublimation was also found by Heymsfield and Iaquinta (2000), Nelson (1998), and Sassen et al. (1994). Similar scattering patterns were recorded by the PPD-2K throughout the CLACE 2013 campaign in general, and the case study period in specific (Fig. 10a), pointing to sublimation of ice crystals as the cause for their imperfect transmission. There are a number of possible reasons for the sublimation which we hypothesise on as follows: Firstly, if the chamber walls are warmer than the ambient air temperature, the ice cover in the evaporation chamber would become patchy. In this case the air entering the evaporation chamber becomes sub-saturated with respect to ice in the vicinity of ice-free wall surfaces (due to the warming influence of the chamber walls on the incoming air) and ice particle sublimation occurs. Secondly if the chamber walls are colder than the cloud the relatively warmer cloud ice crystals sublimate in the presence of the colder chamber wall. Thirdly, the higher saturation vapor pressure over the relatively more curved surfaces of the ice crystal as compared to the flat ice walls of the evaporation chamber (a phenomenon equivalent to the Kelvin effect for liquid droplets) could lead to ice crystal sublimation. Finally, as different facets, edges and structures of the ice crystal surface have different saturation vapour pressures, reshaping of the crystal takes place. Studies on the dynamics of ice crystal growth and sublimation using scanning electron microscopy conducted by Pfalzgraff et al. (2010) give hints on such a process, however temperature and pressure conditions differ significantly from those experienced at the Jungfraujoch. An important note to make in the context of ice crystal reshaping is that we expect an ice particle never to be in a steady state, even in an ice saturated environment. This constitutes a major obstacle for investigating ice microphysics with a sampling system like the ISI in mixed-phase cloud conditions.

4 Conclusions

The ISI, a novel inlet for the selective sampling of small (approximately 5 to 20 µm in aerodynamic diameter) ice crystals in mixed-phase clouds has been designed and developed. Separation of the small ice crystals from other particles found in a mixed-phase cloud (i.e. large crystals, droplets and interstitial particles) is achieved using a modular set of components. An important property of the droplet evaporation unit is that it allows for separation of the liquid and ice phase without physical impaction of the hydrometeors, thus avoiding potential artifacts from ice crystal breakup. In addition to extraction of ice residuals contained in the selectively sampled ice crystals, the ISI provides valuable cloud microphysical information by means of the optical particle spectrometers mounted within the inlet.

Prior to deployment in the field, the performance of the WELAS optical particle spectrometers, as well as the transmission efficiency of the PCVI were characterised in the

AMTD
7, 12481–12515, 2014

laboratory. Subsequently, the ISI was deployed during its first field experiment as part of the CLACE 2013 campaign at the High Altitude Research Station Jungfraujoch. The field campaign provided an opportunity for validation of the operating principle of the droplet evaporation unit. Analysis of hydrometeor size distributions measured by the WELAS sensors shows that droplets are removed very efficiently by the evaporation unit. This was confirmed based on PPD-2K scattering patterns which show that the dominating hydrometeors transmitted by the ISI are ice particles. Partial sublimation of ice crystals in the droplet evaporation unit has however been found to take place. While this does not pose an issue for identification and characterisation of ice residual particles, it does result in lower counting statistics, as well as hindering analysis of the microphysical properties of ice crystals with the PPD-2K downstream of the evaporation unit. Modifications in the design of the droplet evaporation unit for future field measurements will aim to alleviate these issues.

Acknowledgements. This project is funded by the Swiss National Science Foundation (grant 135356), the German Research Foundation (grant SCHN 1140/2-1), MeteoSwiss (GAW-CH program) and the European Research Council (grant 615922-BLACARAT). We thank the International Foundation High Altitude Research Station Jungfraujoch and Gornergrat (HFSJG) for the opportunity to perform experiments on the Jungfraujoch. We would also like to thank Gary Lloyd for providing the PVM data, Stephan Mertes for fruitful discussions and Günther Wehrle for his help with setting up the ISI at the Jungfraujoch.

References

Bohren, C. F. and Huffman, D. R.: Absorption and Scattering of Light by Small Particles, 2007. 12493

Boulter, J. E., Cziczo, D. J., Middlebrook, A. M., Thomson, D. S., and Murphy, D. M.: Design and performance of a pumped counterflow virtual impactor, Aerosol Sci. Tech., 40, 969–976, doi:10.1080/02786820600840984, 2006. 12487, 12495, 12496

Cantrell, W. and Heymsfield, A.: Production of ice in tropospheric clouds: a review, B. Am. Meteorol. Soc., 86, 795–807, doi:10.1175/BAMS-86-6-795, 2005. 12484

Chen, J.-P. and Lamb, D.: Simulation of cloud microphysical and chemical processes using a multicomponent framework. Part II: Microphysical evolution of a wintertime orographic cloud, J. Atmos. Sci., 56, 2293–2312, doi:10.1175/1520-0469(1999)056<2293:SOCMAC>2.0.CO;2, 1999. 12483

Chou, C., Stetzer, O., Weingartner, E., Jurányi, Z., Kanji, Z. A., and Lohmann, U.: Ice nuclei properties within a Saharan dust event at the Jungfraujoch in the Swiss Alps, Atmos. Chem. Phys., 11, 4725–4738, doi:10.5194/acp-11-4725-2011, 2011. 12483

Choularton, T. W., Bower, K. N., Weingartner, E., Crawford, I., Coe, H., Gallagher, M. W., Flynn, M., Crosier, J., Connolly, P., Targino, A., Alfarra, M. R., Baltensperger, U., Sjogren, S., Verheggen, B., Cozic, J., and Gysel, M.: The influence of small aerosol particles on the properties of water and ice clouds, Faraday Discuss., 137, 205–222; discussion 297–318, 2008. 12491

Cozic, J., Mertes, S., Verheggen, B., Cziczo, D. J., Gallavardin, S. J., Walter, S., Baltensperger, U., and Weingartner, E.: Black carbon enrichment in atmospheric ice particle residuals observed in lower tropospheric mixed phase clouds, J. Geophys. Res.-Atmos., 113, D15209, doi:10.1029/2007JD009266, 2008. 12483

Cziczo, D. J., Froyd, K. D., Hoose, C., Jensen, E. J., Diao, M., Zondlo, M. A., Smith, J. B., Twohy, C. H., and Murphy, D. M.: Clarifying the dominant sources and mechanisms of cirrus cloud formation, Science, 340, 1320–1324, doi:10.1126/science.1234145, 2013. 12484

Eames, I., Marr, N., and Sabir, H.: The evaporation coefficient of water: a review, Int. J. Heat Mass Tran., 40, 2963–2973, doi:10.1016/S0017-9310(96)00339-0, 1997. 12490, 12491

Fukuta, N. and Walter, L. A.: Kinetics of hydrometeor growth from a vapor-spherical model, J. Atmos. Sci., 27, 1160–1172, doi:10.1175/1520-0469(1970)027<1160:KOHGFA>2.0.CO;2, 1970. 12490

Glen, A. and Brooks, S. D.: A new method for measuring optical scattering properties of atmospherically relevant dusts using the Cloud and Aerosol Spectrometer with Polarization (CASPOL), Atmos. Chem. Phys., 13, 1345–1356, doi:10.5194/acp-13-1345-2013, 2013. 12494

Heim, M., Mullins, B. J., Umhauer, H., and Kasper, G.: Performance evaluation of three optical particle counters with an efficient “multimodal” calibration method, J. Aerosol Sci., 39, 1019–1031, doi:10.1016/j.jaerosci.2008.07.006, 2008. 12486

Heymsfield, A. J. and Iaquinta, J.: Cirrus crystal terminal velocities, J. Atmos. Sci., 57, 916–938, doi:10.1175/1520-0469(2000)057<0916:CCTV>2.0.CO;2, 2000. 12499

AMTD

7, 12481–12515, 2014

The Ice Selective Inlet

P. Kupiszewski et al.

Title Page

Abstract | Introduction

Conclusions | References

Tables | Figures

◂ | ▸

Back | Close

Full Screen / Esc

Printer-friendly Version

Interactive Discussion

Kärcher, B. and Basko, M. M.: Trapping of trace gases in growing ice crystals, J. Geophys. Res.-Atmos., 109, D22204, doi:10.1029/2004JD005254, 2004. 12486
Kaye, P. H., Hirst, E., Greenaway, R. S., Ulanowski, Z., Hesse, E., DeMott, P. J., Saunders, C., and Connolly, P.: Classifying atmospheric ice crystals by spatial light scattering, Opt. Lett., 33, 1545–1547, doi:10.1364/OL.33.001545, 2008. 12486, 12487, 12497, 12498
Kreidenweis, S. M., Walcek, C. J., Feingold, G., Gong, W., Jacobson, M. Z., Kim, C.-H., Liu, X., Penner, J. E., Nenes, A., and Seinfeld, J. H.: Modification of aerosol mass and size distribution due to aqueous-phase SO2 oxidation in clouds: comparisons of several models, J. Geophys. Res.-Atmos., 108, D7, 4213, doi:10.1029/2002JD002697, 2003. 12491
Kulkarni, G., Pekour, M., Afchine, A., Murphy, D. M., and Cziczo, D. J.: Comparison of experimental and numerical studies of the performance characteristics of a pumped counterflow virtual impactor, Aerosol Sci. Tech., 45, 382–392, doi:10.1080/02786826.2010.539291, 2011. 12487, 12495, 12496
Laaksonen, A., Vesala, T., Kulmala, M., Winkler, P. M., and Wagner, P. E.: Commentary on cloud modelling and the mass accommodation coefficient of water, Atmos. Chem. Phys., 5, 461–464, doi:10.5194/acp-5-461-2005, 2005. 12491
Lohmann, U.: A glaciation indirect aerosol effect caused by soot aerosols, Geophys. Res. Lett., 29, 4, 11-1–11-4, doi:10.1029/2001GL014357, 2002. 12484
Lohmann, U. and Feichter, J.: Global indirect aerosol effects: a review, Atmos. Chem. Phys., 5, 715–737, doi:10.5194/acp-5-715-2005, 2005. 12483
Lowe, P. R. and Ficke, J. M.: The computation of saturation vapor pressure, Technical Paper 4-74, Tech. rep., Environmental Prediction Research Facility, Naval Postgraduate School, Monterey, CA, 1974. 12488, 12507
Marécal, V., Pirre, M., Rivière, E. D., Pouvesle, N., Crowley, J. N., Freitas, S. R., and Longo, K. M.: Modelling the reversible uptake of chemical species in the gas phase by ice particles formed in a convective cloud, Atmos. Chem. Phys., 10, 4977–5000, doi:10.5194/acp-10-4977-2010, 2010. 12486
Marek, R. and Straub, J.: Analysis of the evaporation coefficient and the condensation coefficient of water, Int. J. Heat Mass Tran., 44, 39–53, doi:10.1016/S0017-9310(00)00086-7, 2001. 12490
Mertes, S., Verheggen, B., Walter, S., Connolly, P., Ebert, M., Schneider, J., Bower, K. N., Cozic, J., Weinbruch, S., Baltensperger, U., and Weingartner, E.: Counterflow virtual impactor based collection of small ice particles in mixed-phase clouds for the physico-chemical char-

AMTD
7, 12481–12515, 2014

acterization of tropospheric ice nuclei: sampler description and first case study, Aerosol Sci. Tech., 41, 848–864, doi:10.1080/02786820701501881, 2007. 12484, 12485, 12496

Möhler, O., Büttner, S., Linke, C., Schnaiter, M., Saathoff, H., Stetzer, O., Wagner, R., Krämer, M., Mangold, A., Ebert, V., and Schurath, U.: Effect of sulfuric acid coating on heterogeneous ice nucleation by soot aerosol particles, J. Geophys. Res.-Atmos., 110, D11210, doi:10.1029/2004JD005169, 2005. 12499

Mosimann, L., Weingartner, E., and Waldvogel, A.: An analysis of accreted drop sizes and mass on rimed snow crystals, J. Atmos. Sci., 51, 1548–1558, doi:10.1175/1520-0469(1994)051<1548:AAOADS>2.0.CO;2, 1994. 12486

Myhre, G., Shindell, D., Bréon, F.-M., Collins, W., Fuglestvedt, J., Huang, J., Koch, D., Lamarque, J.-F., Lee, D., Mendoza, B., Nakajima, T., Robock, A., Stephens, G., Takemura, T., and Zhang, H.: Anthropogenic and natural radiative forcing, in: Climate Change 2013: The Physical Science Basis. Contribution of Working Group I to the Fifth Assessment Report of the Intergovernmental Panel on Climate Change, chap. 8, Cambridge University Press, Cambridge, UK and New York, NY, USA, 659–740, 2013. 12483

Nelson, J.: Sublimation of ice crystals, J. Atmos. Sci., 55, 910–919, doi:10.1175/1520-0469(1998)055<0910:SOIC>2.0.CO;2, 1998. 12499

Penner, J. E.: Climate change: the cloud conundrum, Nature, 432, 962–963, doi:10.1038/432962a, 2004. 12483

Pfalzgraff, W. C., Hulscher, R. M., and Neshyba, S. P.: Scanning electron microscopy and molecular dynamics of surfaces of growing and ablating hexagonal ice crystals, Atmos. Chem. Phys., 10, 2927–2935, doi:10.5194/acp-10-2927-2010, 2010. 12500

Pound, G. M.: Selected values of evaporation and condensation coefficients for simple substances, J. Phys. Chem. Ref. Data, 1, 135–146, doi:10.1063/1.3253096, 1972. 12490

Prenni, A. J., DeMott, P. J., Twohy, C., Poellot, M. R., Kreidenweis, S. M., Rogers, D. C., Brooks, S. D., Richardson, M. S., and Heymsfield, A. J.: Examinations of ice formation processes in Florida cumuli using ice nuclei measurements of anvil ice crystal particle residues, J. Geophys. Res.-Atmos., 112, D10221, doi:10.1029/2006JD007549, 2007. 12484

Pruppacher, H. R. and Klett, J. D.: Microphysics of Clouds and Precipitation, 2nd ed., Kluwer Academic Publishers, 1997. 12483

Rosati, B., Wehrle, G., Zieger, P., Gysel, M., Baltensperger, U., and Weingartner, E.: The white-light humidified optical particle spectrometer (WHOPS) – a novel airborne sys-

AMTD

7, 12481–12515, 2014

The Ice Selective Inlet

P. Kupiszewski et al.

tem to characterize aerosol hygroscopicity, Atmos. Meas. Tech. Discuss., 7, 7321–7366, doi:10.5194/amtd-7-7321-2014, 2014. 12486

Sassen, K., Knight, N. C., Takano, Y., and Heymsfield, A. J.: Effects of ice-crystal structure on halo formation: cirrus cloud experimental and ray-tracing modeling studies, Appl. Optics, 33, 4590–4601, doi:10.1364/AO.33.004590, 1994. 12499

Seinfeld, J. H. and Pandis, S. N.: Atmospheric Chemistry and Physics: From Air Pollution to Climate Change, 2nd Edn., Wiley, 2006. 12489

Shaw, R. A. and Lamb, D.: Experimental determination of the thermal accommodation and condensation coefficients of water, J. Chem. Phys, 111, 10659–10663, doi:10.1063/1.480419, 1999. 12490

Sun, Z. and Shine, K. P.: Studies of the radiative properties of ice and mixed-phase clouds, Q. J. Roy. Meteor. Soc., 120, 111–137, doi:10.1002/qj.49712051508, 1994. 12483

Twohy, C. H. and Poellot, M. R.: Chemical characteristics of ice residual nuclei in anvil cirrus clouds: evidence for homogeneous and heterogeneous ice formation, Atmos. Chem. Phys., 5, 2289–2297, doi:10.5194/acp-5-2289-2005, 2005. 12484

Vochezer, P., Wagner, R., Järvinen, E., Abedelmonem, A., Kupiszewski, P., and Schnaiter, M.: In situ characterization of mixed phase clouds using the Small Ice Detector (SID-3) and the Particle Phase Discriminator (PPD-2K), Atmos. Meas. Tech. Discuss., in preparation, 2014. 12487, 12498

Weingartner, E., Nyeki, S., and Baltensperger, U.: Seasonal and diurnal variation of aerosol size distributions ($10 < D < 750$ nm) at a high-alpine site (Jungfraujoch 3580 m asl), J. Geophys. Res.-Atmos., 104, 26809–26820, doi:10.1029/1999JD900170, 1999. 12496

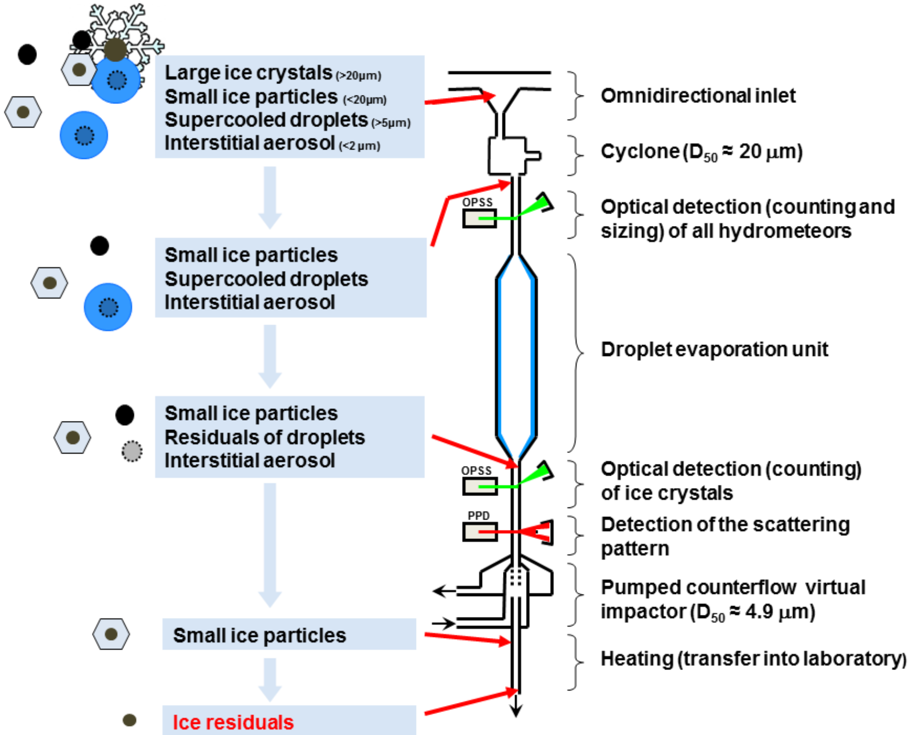

Figure 1. Sketch of the Ice Selective Inlet. The particulate matter contained within the sample flow is visualized on the left-hand side of the figure.

AMTD
7, 12481–12515, 2014

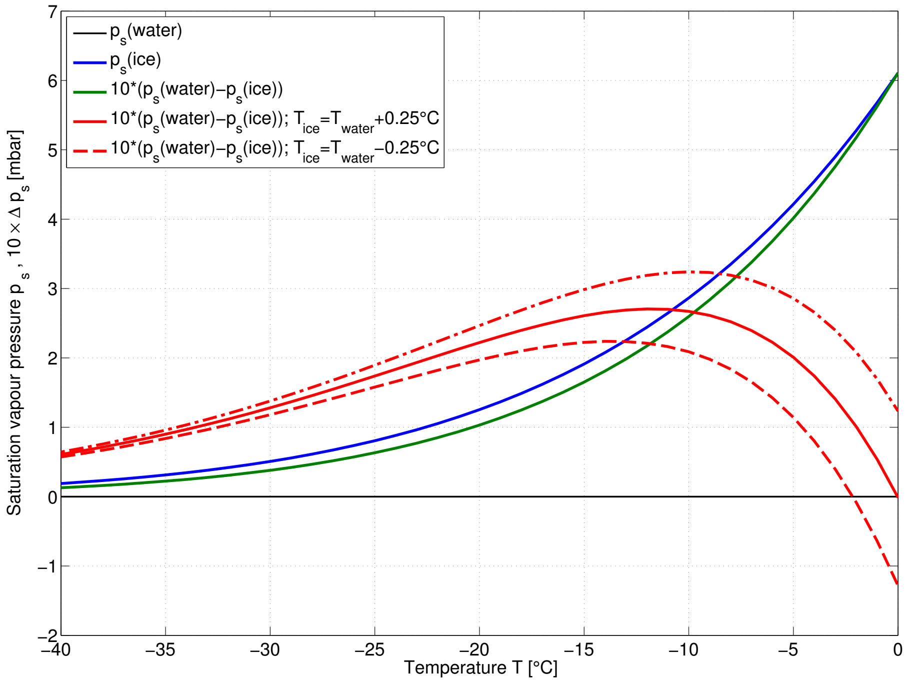

Figure 2. Saturation vapour pressures over bulk liquid water (blue curve) and ice (green curve) surfaces as a function of temperature (the parametrisations used for the saturation vapour pressures over water and ice are based on Lowe and Ficke, 1974). The difference (multiplied by a factor of ten) in the saturation vapour pressures of water and ice is given by the red curve. The difference (multiplied by a factor of ten) in the saturation vapour pressures of water and ice when the ice temperature (T_{ice}) is 0.25 °C higher and lower than the water temperature (T_{water}) is given by the dashed and dotted red lines respectively.

AMTD
7, 12481–12515, 2014

The Ice Selective Inlet

P. Kupiszewski et al.

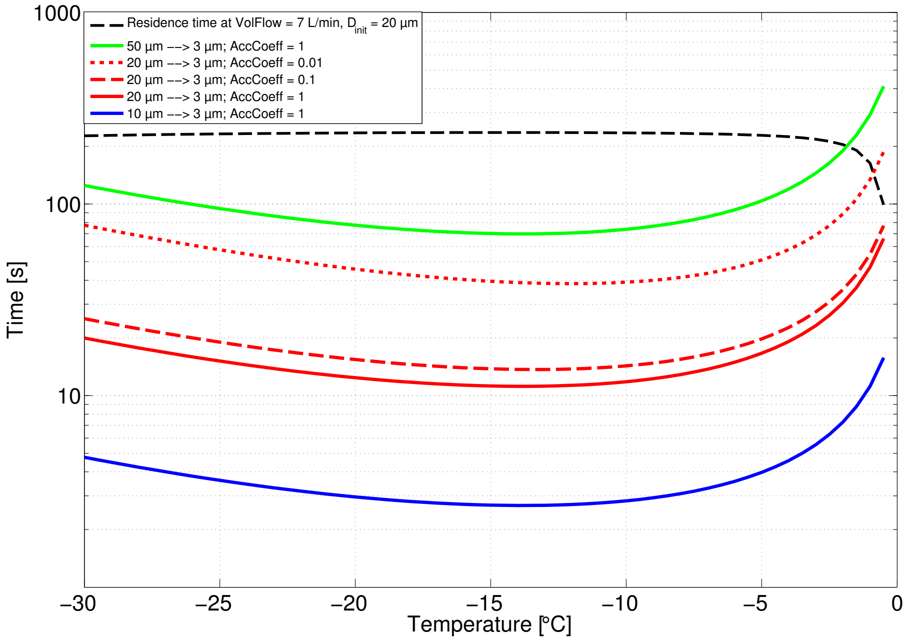

Figure 3. Evaporation times of cloud droplets in the evaporation unit for different droplet start and end diameters, and different mass accommodation coefficients, as a function of temperature at a pressure of $p = 658.61$ hPa. The average residence time as a function of temperature based on the dimensions of the droplet evaporation unit and a sample flow of 7 L min^{-1} is shown by the dotted black line.

AMTD
7, 12481–12515, 2014

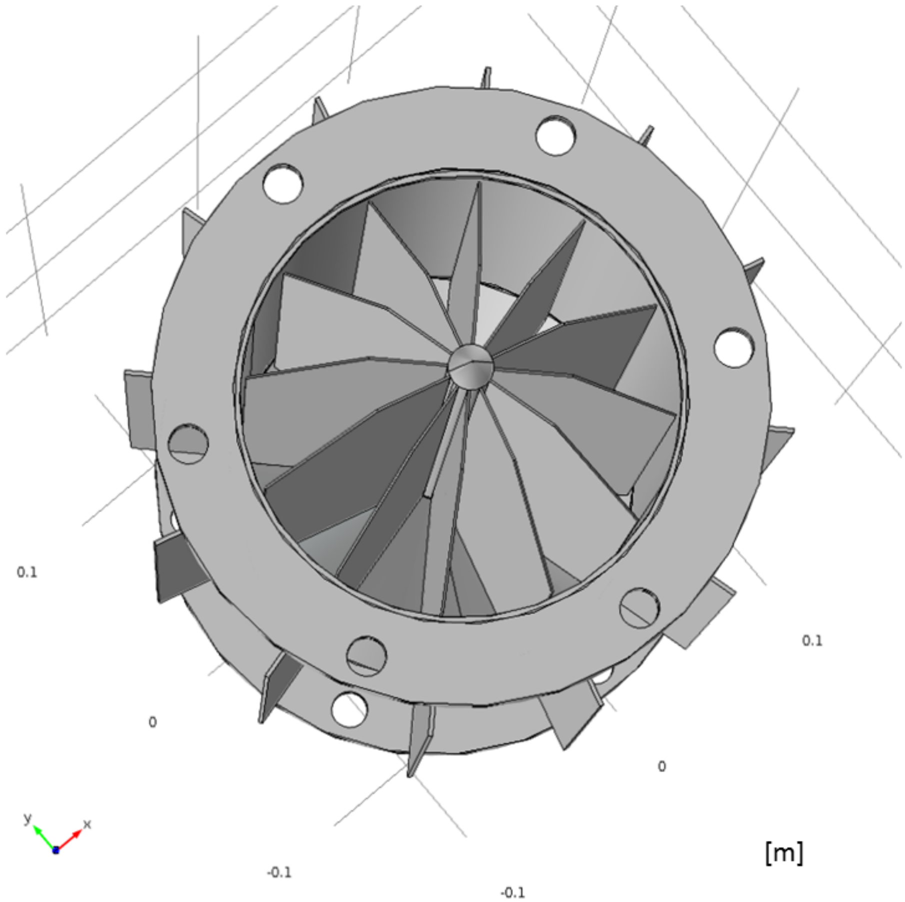

Figure 4. The internal structure of the droplet evaporation unit as seen from above.

AMTD
7, 12481–12515, 2014

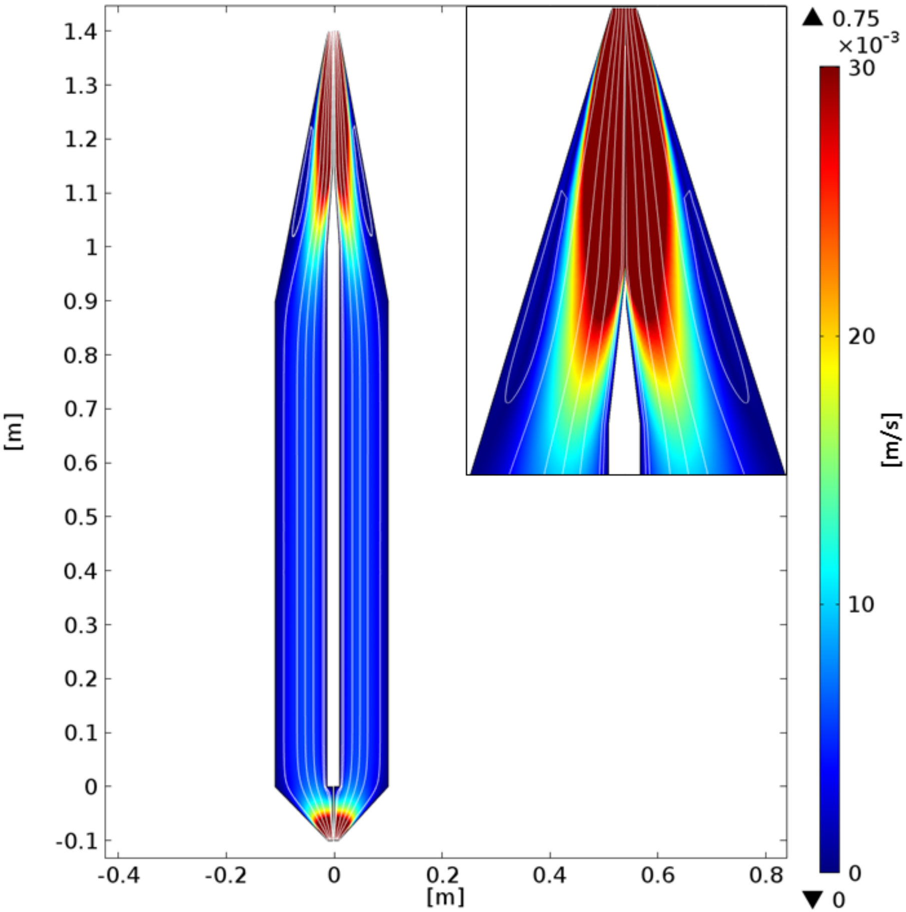

Figure 5. A 2-D cross-section of the droplet evaporation unit showing the air streamlines and velocity field, calculated using Comsol 4.2a. An enlargement (not to scale) of the upper cone section of the evaporation unit is shown in the inset.

AMTD
7, 12481–12515, 2014

The Ice Selective Inlet

P. Kupiszewski et al.

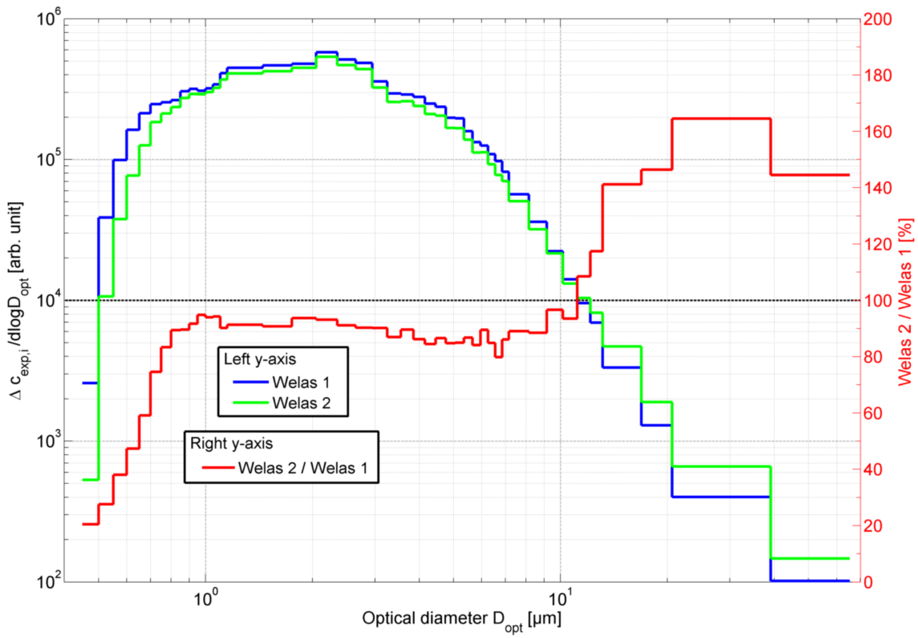

Figure 6. Intercomparison of the ISI WELAS Optical Particle Size Spectrometers. Note: $\Delta c_{\mathrm{exp},i}$ is the number count of particles with diameters that fall into size bin *i*.

Discussion Paper | Discussion Paper | Discussion Paper | Discussion Paper |

AMTD

7, 12481–12515, 2014

The Ice Selective Inlet

P. Kupiszewski et al.

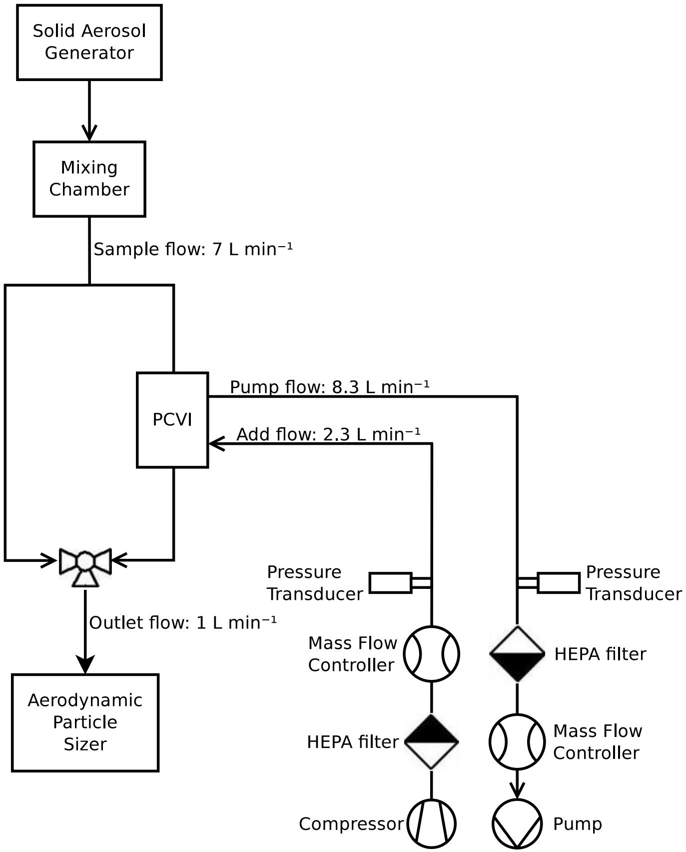

Figure 7. Schematic of laboratory setup for the pumped counterflow virtual impactor (PCVI) transmission efficiency tests.

AMTD
7, 12481–12515, 2014

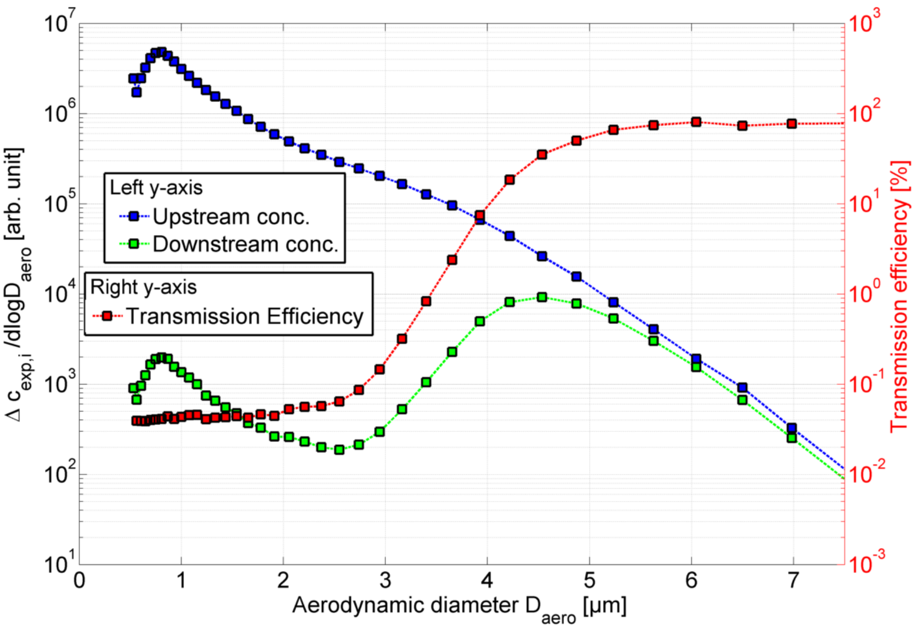

Figure 8. Transmission efficiency of the BMI PCVI, with flows of $7\,\mathrm{L\,min^{-1}}$ (sample flow), $8.3\,\mathrm{L\,min^{-1}}$ (pump flow), $2.3\,\mathrm{L\,min^{-1}}$ (add flow) and $1\,\mathrm{L\,min^{-1}}$ (outlet flow), as measured by a TSI model 3321 Aerodynamic Particle Sizer. Note: $\Delta c_{\mathrm{exp},i}$ is the number count of particles with diameters that fall into size bin i.

AMTD
7, 12481–12515, 2014

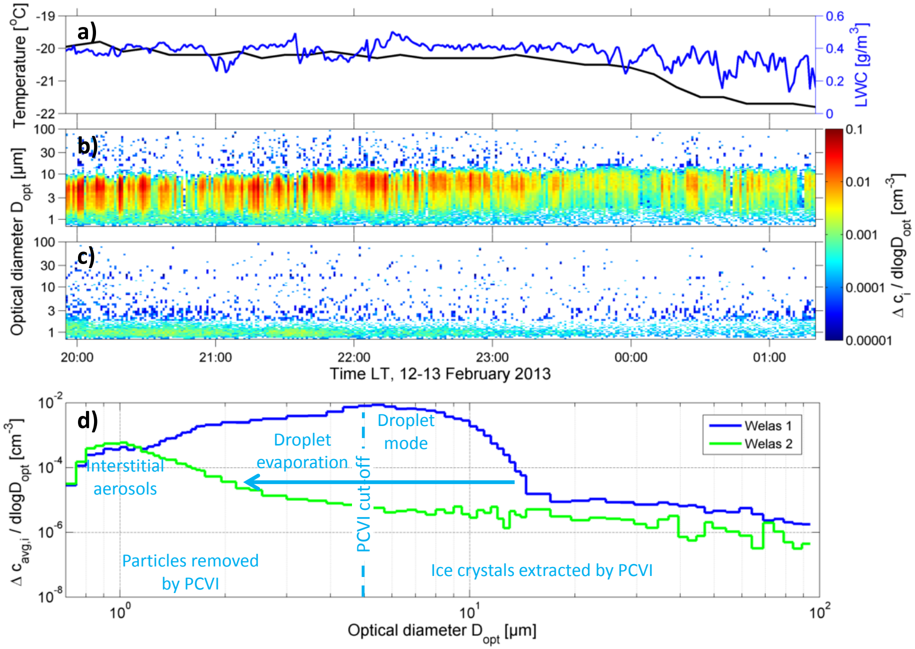

Figure 9. Measurements of liquid water content, air temperature and particle number size distributions during the case study period of 19:55 LT, 12 February 2013 to 01:20 LT, 13 February 2013. Panel **(a)** shows air temperature (black curve) and liquid water content (blue curve), panels **(b)** and **(c)** show time resolved size distributions measured with the upper and lower ISI WELAS 2500 sensors respectively and panel **(d)** shows average size distributions for the case study period from the two WELAS sensors with an overlaid description of the processes at work in the ISI, and the resulting size distribution characteristics. Note: Δc_i is the number concentration of particles with diameters that fall into size bin *i*; $\Delta c_{\text{avg},i}$ is the case study average number concentration of particles with diameters that fall into size bin *i*.

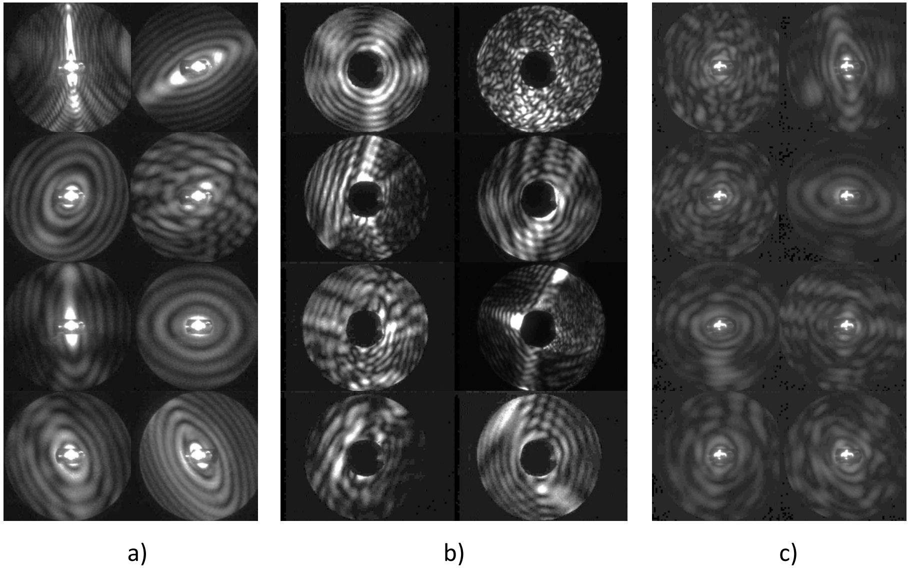

Figure 10. Randomly selected scattering patterns recorded by the PPD-2K downstream of the ISI during CLACE 2013 between 19:55 LT, 12 February 2013 and 01:20 LT, 13 February 2013 **(a)**, by the SID-3 directly sampling ambient air during CLACE 2013 on the 12 February 2013 **(b)** and by the PPD-2K directly connected to the AIDA cloud chamber during the final stage of an ice cloud experiment **(c)**. The patterns display the distribution of scattered light measured between 0 and $\sim 26^{\circ}$ relative to the forward direction. The black area in the centre of the SID-3 scattering patterns is caused by absorption of light scattered between 0 and $\sim 5^{\circ}$ by the beam dump of the SID-3. The bar in the center of the PPD-2K scattering patterns is caused by the beam dump of the PPD-2K.

AMTD
7, 12481–12515, 2014

The Ice Selective Inlet

P. Kupiszewski et al.